

De Haas-van Alphen oscillations in the compensated organic metal α -'pseudo- κ '-(ET)₄H₃O[Fe(C₂O₄)₃](C₆H₄Br₂)

Alain Audouard^{1a}, Jean-Yves Fortin^{2b}, Vladimir N. Laukhin^{3,4}, David Vignolles¹, Tatyana G. Prokhorova⁵, Eduard B. Yagubskii⁵, and Enric Canadell⁴

¹ Laboratoire National des Champs Magnétiques Intenses (UPR 3228 CNRS, INSA, UJF, UPS) 143 avenue de Rangueil, F-31400 Toulouse, France.

² Institut Jean Lamour, Département de Physique de la Matière et des Matériaux, CNRS-UMR 7198, Vandoeuvre-les-Nancy, F-54506, France.

³ Institució Catalana de Recerca i Estudis Avançats (ICREA), 08010 Barcelona, Spain.

⁴ Institut de Ciència de Materials de Barcelona, CSIC, Campus de la UAB, 08193, Bellaterra, Spain.

⁵ Institute of Problems of Chemical Physics, Russian Academy of Sciences, 142432 Chernogolovka, MD, Russia

Received: date / Revised version: date

Abstract. Field-, temperature- and angle-dependent Fourier amplitude of de Haas-van Alphen (dHvA) oscillations are calculated for compensated two-dimensional (2D) metals with textbook Fermi surface (FS) composed of one hole and two electron orbits connected by magnetic breakdown. It is demonstrated that, taking into account the opposite sign of electron and hole orbits, a given Fourier component involves combination of several orbits, the contribution of which must be included in the calculations. Such FS is observed in the strongly 2D organic metal α -'pseudo- κ '-(ET)₄H₃O[Fe(C₂O₄)₃](C₆H₄Br₂), dHvA oscillations of which have been studied up to 55 T for various directions of the magnetic field with respect to the conducting plane. Calculations are in good quantitative agreement with the data.

PACS. 71.18.+y Fermi surface: calculations and measurements; effective mass, g factor – 71.20.Rv Polymers and organic compounds

1 Introduction

Provided that no phase transition occurs as the temperature is lowered, Fermi surface (FS) of two-dimensional (2D) organic metals is generally rather simple and achieve model systems for quantum oscillations physics. Indeed, in the numerous cases where the compound possesses two carriers (generally holes) per unit cell, the FS originates from a single orbit with an area equal to that of the first Brillouin zone [1]. In an extended zone scheme, these orbits overlap either along (i) one or (ii) two directions yielding in magnetic field either (i) the model linear chain of orbits coupled by magnetic breakdown (MB) proposed by Pippard in the early sixties [2,3] for which all the orbits are of the same (hole) type or (ii) a set of compensated electron- and hole-type orbits (i.e. the sum of the hole-type orbits cross section is equal to that of the electron-type orbits).

The former case (i) has been widely studied: it is known that quantum oscillations spectra are strongly affected by field-induced chemical potential oscillations yielding many frequency combinations, the field and temperature dependence of which cannot be accounted for by the Lifshitz-Kosevich (LK) formula [4,5,6]. In contrast, to our best knowledge, the second case (ii) has only received little attention up to now even though MB between hole- and electron-type orbits is relevant, for instance, for recently studied oxide superconductors [7,8,9]. Numerical resolution of the grand potential equation for the case (ii) reveals

that chemical potential oscillations are strongly damped for compensated orbits, even in the case of 2D metals [10, 11]. As a consequence, contrary to case (i), the LK formula is predicted to account for the field and temperature dependence of the oscillations amplitude in case (ii). However, depending on the MB probability and taking into account the opposite sign of electron and hole orbits, a given Fourier component can involve combinations of an infinite set of orbits, the contribution of which must be included in the Fourier amplitudes calculation. From the experimental side, only few quasi-2D compensated metals have been synthesized yet. Such FS are observed in e.g. (BEDO-TTF)₂ReO₄·H₂O [12] (where BEDO-TTF stands for the bis-ethylenedioxy-tetrathiafulvalene molecule) and, more recently synthesized, (ET)₄H₃O[Fe(C₂O₄)₃]·Solv (where ET stands for the bis-ethylenedithio-tetrathiafulvalene molecule and Solv is an organic solvent) [13,14].

As reported in Fig. 1(a), the unit cell of α -'pseudo- κ '-(ET)₄H₃O[Fe(C₂O₄)₃]·(C₆H₄Br₂) [13] contains two different donor planes with different packing. One of them, with a 'pseudo- κ ' structure is insulating while the other with an α -type structure is metallic. As a consequence, spacing between conducting layers is as large as 3.64 nm, ensuring negligibly small interlayer transfer integral, hence avoiding effects due to FS corrugation [15]. According to band structure calculations, the FS of the metallic plane, displayed in Fig. 1(b), is composed of two electron-type and one hole-type compensated orbits (i.e. the hole orbit area is twice the electron orbits area). In the extended zone scheme, this set of three orbits is isolated from the other

^a e-mail: alain.audouard@lncmi.cnrs.fr

^b e-mail: fortin@ijl.nancy-universite.fr

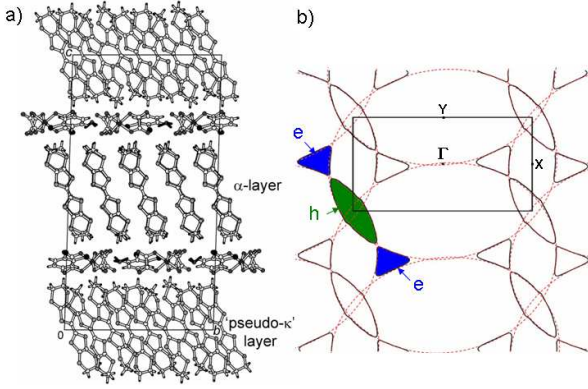


Fig. 1. (color on line) (a) Crystal structure of α' -pseudo- κ' -(ET) $_4\text{H}_3\text{O}[\text{Fe}(\text{C}_2\text{O}_4)_3] \cdot (\text{C}_6\text{H}_4\text{Br}_2)$. α -type and 'pseudo- κ' '-type layers are conducting and insulating, respectively. (b) Fermi surface relevant to the α -type layers, according to Zorina et al.[13]. Blue and green areas mark electron- and hole-type orbits, respectively. Ellipses in dashed lines mark the orbits from which the Fermi surface originates. Labels Γ , X and Y refer to the $(0, 0)$, $(a^*/2, 0)$ and $(0, b^*/2)$ points of the first Brillouin zone, displayed as a rectangle in solid line.

sets. In other words, we are not dealing with a network of coupled orbits. In contrast, each of the orbits within a set is liable to be connected to the other by MB. This feature is shared by the FS studied in Ref. [10], which is composed of one hole and one electron compensated orbit.

The aim of this paper is, in the first step, to provide calculation of the Fourier amplitudes of de Haas-van Alphen (dHvA) oscillations spectra for the FS of Fig. 1(b). In the second step, magnetic torque oscillations of α' -pseudo- κ' -(ET) $_4\text{H}_3\text{O}[\text{Fe}(\text{C}_2\text{O}_4)_3] \cdot (\text{C}_6\text{H}_4\text{Br}_2)$, yielding dHvA spectra, are studied in magnetic fields up to 55 T. Whereas magnetoresistance data of this organic metal, measured in magnetic fields below 16 T reveal only one frequency attributed to the hole orbit [13], the two frequencies cor-

responding to electron and hole orbits area are observed. It is shown that the field and temperature dependence of the Fourier amplitudes are in agreement with the reported calculations.

2 Experimental

Crystals were synthesized by electrocrystallization technique as reported by Zorina et al.[13]. Two crystals denoted as crystal #1 and #2 hereafter were studied. Their approximate dimensions were $0.12 \times 0.1 \times 0.04 \text{ mm}^3$. Magnetic torque was measured with a commercial piezoresistive microcantilever, in pulsed magnetic fields of up to 55 T with a pulse decay duration of 0.32 s. Variations of the cantilever piezoresistance were measured in the temperature range from 1.4 K to 4.2 K with a Wheatstone bridge with an ac excitation at a frequency of 63 kHz. The angle between the normal to the conducting plane and the magnetic field direction was $\theta = 15^\circ$ and 32° for crystal #1 while θ was varied from 15° to 71° thanks to a rotating sample holder for crystal #2.

3 Calculations of the Fourier amplitudes

In the framework of the Lifshitz-Kosevich and Falicov-Stachowiak models [3,16], the oscillatory part of the magnetization M_{osc} for a set of 2D orbits η can be written as

$$M_{osc} = - \sum_{\eta} \sum_p \frac{F_{\eta}}{\pi} A_{p\eta} \sin(2\pi p \frac{F_{\eta}}{B \cos \theta}) \quad (1)$$

where θ is the angle between the normal to the conducting plane and the field direction. The index η stands for all the closed orbits allowed by the FS topology, including MB orbits, with fundamental frequencies F_η . They do not include orbits which can be associated with an harmonic of a simpler trajectory, the latter being accounted for by the index pF_η (with $p > 1$) where p is the harmonic order. The amplitude $A_{p\eta}$ of the Fourier component with frequency pF_η depend on parameters such as temperature, magnetic field, effective masses (m_η), Dingle temperatures ($T_{D\eta}$), MB field (B_0), and effective Landé factors (g_η^*). These amplitudes can be expressed as $A_{p\eta} = (-1)^{ps_\eta} R_{p\eta}^{MB} R_{p\eta} / (pm_\eta)$. MB damping factor is given by $R_{p\eta}^{MB} = C_{p\eta} (ip_0)^{pt_\eta} q_0^{pb_\eta}$, where $C_{p\eta}$ is the symmetry factor of the orbit $p\eta$, t_η and b_η are the number of tunnelings and reflections, respectively, encountered by a quasi-particle during its path and $2s_\eta$ is the number of turning points around the orbit η . The tunneling and reflection probabilities at a MB junction are given, in agreement with the Chambers approximation, by $p_0^2 = \exp(-B_0/B \cos \theta)$ and $q_0^2 = 1 - p_0^2$, respectively [17]. The damping factor $R_{p\eta}$ can be written as the product of thermal, Dingle and spin damping factors ($R_{p\eta} = R_{p\eta}^T R_{p\eta}^D R_{p\eta}^s$) which are given by $R_{p\eta}^T = X_{p\eta} / \sinh(X_{p\eta})$, $R_{p\eta}^D = \exp(-u_0 T_{D\eta} p m_\eta / B \cos \theta)$, and $R_{p\eta}^s = \cos(p\pi g_\eta^* m_\eta / 2 \cos \theta)$, respectively, where $X_{p\eta} = u_0 T p m_\eta / B \cos \theta$ and $u_0 = 2\pi^2 k_B^2 m_e / e\hbar$.

In the case of the FS of Fig.1(b), which is modeled by Fig. 2, and owing to the orbits compensation predicted by band structure calculations, each electron (e) and hole (h) orbit contributes to the dHvA oscillations

spectrum with the frequency F_e and $F_h = 2F_e$, respectively. Besides, MB orbits composed of several individual orbits ($\eta = n_e e + n_h h$) are also liable to contribute to the spectrum. Indeed, all contributing trajectories for a given frequency are accounted for by considering the amplitude and phase variation $\exp(iS_\eta) = \exp[2i\pi h \mathcal{A}_\eta / eB]$ of the wave-function, where \mathcal{A}_η is the area of the trajectory in the Brillouin zone, which is directly identified to the frequency $F_\eta = |\mathcal{A}_\eta| h / e$. Taking into account the opposite sign of electron and hole surface area, $S_{n_e e + n_h h} = n_e S_e + n_h S_h$ with $S_h = -2S_e$, all Fourier components with frequencies $F_{n_e e + n_h h} = |n_e F_e - n_h F_h| = |n_e - 2n_h| F_e$, and effective masses $m_{n_e e + n_h h} = n_h m_h + n_e m_e$ [3, 16], where n_e and n_h are the (positive) numbers of electron and hole orbits involved, contribute. Therefore, the dominant frequencies F_e , $2F_e = F_h$ and $3F_e$ we will consider in the following, arise from infinite orbits combinations with $n_e = 2n_h \pm 1$, $n_e = 2n_h \pm 2$ and $n_e = 2n_h \pm 3$, respectively. To obtain the amplitude of these Fourier components, the Fermi surface is modeled in Fig. 2 by a linear finite chain of e and h orbits.

To count all the allowed paths from one of the arbitrary starting and ending points $\alpha, \bar{\beta}, \beta, \gamma$ in Fig. 2, we consider paths of length n , where n is an integer corresponding to the number of elementary steps from one point to another that form and define the complete closed trajectory. Turning points are located at the arrows in Fig. 2 and going through one of these is tantamount to adding a factor i in the wave-function amplitude. We introduce the vector amplitude $|\alpha, \bar{\beta}, \beta, \gamma\rangle$ corresponding to the state of

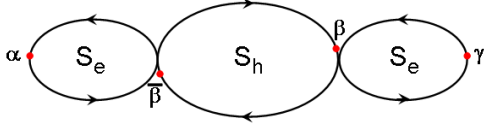


Fig. 2. Compensated Fermi surface with classical representation of the quasi-particle orbits. Phase variation of the wavefunction is given by $\exp(iS_e)$ around the electronic orbit e and $\exp(iS_h)$ around the hole orbit h , where $S_{e(h)}$ is the electron (hole) surface area. Either magnetic breakdown occurs with the probability amplitude ip_0 between two orbits or reflection is allowed with the probability amplitude $q_0 = (1 - p_0^2)^{1/2}$.

the quasi-particle. Any closed path is therefore defined by its length n and its starting point and state s_0 among the set $(\alpha, \bar{\beta}, \beta, \gamma)$. Initially the state $|s_0\rangle$ is filled with zeroes except for the component corresponding to s_0 , for example $|\alpha\rangle = |1, 0, 0, 0\rangle$. We then define each step factor of the trajectory by moving from one point among the set $(\alpha, \bar{\beta}, \beta, \gamma)$ to the next one, by following the direction imposed by the field, with the adequate changes in the phase and amplitude. For example, as shown in Fig. 2, $\beta = -ip_0\alpha \exp(iS_e/2 + iS_h/2) + iq_0\bar{\beta} \exp(iS_h/2)$. Introducing parameters $x = \exp(iS_e/2)$ and $y = \exp(iS_h/2)$, with $y = 1/x^2$, we can write a transfer matrix for all the elementary steps on the Fermi surface:

$$T(x, y) = \begin{pmatrix} -q_0x^2 & -ip_0xy & 0 & 0 \\ 0 & 0 & iq_0y & -p_0x \\ -p_0x & iq_0y & 0 & 0 \\ 0 & 0 & -ip_0xy & -q_0x^2 \end{pmatrix}$$

Since we consider closed paths and conserved current, the output vector is the same as the input vector $|s_0\rangle$.

Then the number of all possible paths of length n and starting from a point s_0 is given by the number $\langle s_0|T(x, y)^n|s_0\rangle$.

The generalized damping factor $A_{p\eta}$ in Eq. (1) is computed for all possible orbit combinations contributing to the same frequency pF_η . The combinatorial factor $(-1)^{ps_\eta} R_{p\eta}^{MB}$ in $A_{p\eta}$, combining the different ways of drawing the orbits $p\eta$ on the FS, is precisely defined as the coefficient of $x^{2n_e}y^{2n_h}$, as well as $x^{-2n_e}y^{-2n_h}$, in the following polynomial function

$$A(x, y) = \int_0^1 \frac{dz}{z} \sum_{s_0} \sum_{n \geq 0} W_{s_0} \langle s_0|T^n(\sqrt{z}x, zy)|s_0\rangle \quad (2)$$

weighted by damping factors for each orbit, and corresponding to integers (n_e, n_h) . W_{s_0} is the *weight* of the point s_0 in the quasi-particle path. We will take $W_\alpha = W_\gamma = 1$ and $W_\beta = W_{\bar{\beta}} = 1/2$. Indeed points β and $\bar{\beta}$ are equivalent in the sense that they define the same set of paths and belong to the same orbit. Finally, the integration over z is performed so that to remove the number of cyclic permutations $n_e + 2n_h$ of the same fundamental orbit by adding a compensatory factor $1/(n_e + 2n_h)$, and to take into account the harmonics coefficients with a weighting factor $1/p$. Each path can be simply decomposed using e (or x) for a portion of trajectory around the electron orbits, and \sqrt{h} (or y) around the hole orbit, and z is added for each e or \sqrt{h} encountered on the trajectory. For example the orbit $ee\sqrt{h}e\sqrt{h}$ (corresponding to $n_e = 3$, $n_h = 1$) with effective mass $3m_e + m_h$ and phase S_e (corresponding to the frequency F_e) has a weight proportional to $10p_0^4q_0/5 = 2p_0^4q_0$ (the factor $5 = n_e + 2n_h$ is the number of cyclic permutations of the same orbit

$ee\sqrt{h}e\sqrt{h} = e\sqrt{h}e\sqrt{h}e = \dots$). It is different from the orbit $ee\sqrt{h}\sqrt{h}e$ for example, which has a weight proportional to $-2p_0^3q_0^2$. We find that the first three amplitudes can be written as

$$A_e = -\frac{2q_0}{m_e}R_e - \frac{2p_0^2q_0}{m_e + m_h}R_{e+h} + \frac{2[p_0^4q_0 - p_0^2q_0^3]}{3m_e + m_h}R_{3e+h} + \dots, \quad (3)$$

$$A_{2e} = \frac{q_0^2}{2m_e}R_{2e} - \frac{q_0^2}{m_h}R_h + \frac{3p_0^4q_0^2 - 2p_0^2q_0^4}{2(m_e + m_h)}R_{2e+2h} + \frac{2p_0^2q_0^4 - 3p_0^4q_0^2}{4m_e + m_h}R_{4e+h} + \dots \quad (4)$$

$$A_{3e} = -\frac{2q_0^3}{9m_e}R_{3e} + \frac{2p_0^2q_0^3}{m_e + 2m_h}R_{e+2h} + \dots \quad (5)$$

where $R_{p\eta} = R_{p\eta}^T R_{p\eta}^D R_{p\eta}^s$. As an example, the first term $-(2q_0^3/9m_e)R_{3e}$ of A_{3e} in Eq. 5, comes from the third harmonics of the e orbit. Indeed, according to Eq. 1, this factor is given by $F_e(-2q_0^3)R_{3e}/(3m_e)$ which can be rewritten as $3F_e(-2q_0^3)R_{3e}/(9m_e)$. Magnetization can then be expanded as

$$M_{osc} = -\frac{F_e}{\pi}A_e \sin\left(2\pi\frac{F_e}{B}\right) - \frac{2F_e}{\pi}A_{2e} \sin\left(2\pi\frac{2F_e}{B}\right) - \frac{3F_e}{\pi}A_{3e} \sin\left(2\pi\frac{3F_e}{B}\right) + \dots \quad (6)$$

Examples of Fourier spectra deduced from Eq. 6 are reported in Fig. 3(a) for various temperatures and MB fields. Landé factors ($g_e^* = 2$, $g_h^* = 2$) and effective masses ($m_e = 1$, $m_h = 1$), which otherwise are close to those deduced from the data reported in the next section, are chosen

so that the absolute value of the spin damping factors is equal to 1 ($|R_{p\eta}^s|=1$) in order to avoid any spurious effect due to spin-zero phenomenon. First, A_{3e} is always small compared to A_e and A_{2e} . Corresponding field-dependent amplitudes A_{2e} are given in Figs. 3(b), (c), (d). Despite the effective mass m_η of a given η orbit increases as the number of individual orbits involved increases, a clear contribution of the orbits $2e$, $2e + 2h$ and $4e + h$ to the amplitude is observed in Fig. 3(b). Their relative contributions decrease as the Dingle temperatures (not shown), the temperature (see Fig. 3(c)) and the MB field (see Fig. 3(d)) increase which may lead to errors in effective mass determination [11]. Contribution of the orbit $2e$ is substantial in any case, which indicates that this orbit needs to be considered, even in the case of large MB field, scattering rate and temperature, for correct data analysis. In contrast, complex orbits such as $2e + 2h$ have significant contribution for clean compounds with moderate MB field at low temperature, only. Similar conclusions can be derived regarding the component with frequency F_e for which the contribution of $e + h$ is always significant in the range explored, except for large MB fields, while $3e + h$ is negligible at high temperature and large scattering rate. Of course, all the considered amplitudes also depend on the field- and temperature-independent spin damping factor $R_{p\eta}^s$ through the product $g_\eta^*m_\eta$.

4 Results and discussion

This section is devoted to de Haas-van Alphen oscillations of α -'pseudo- κ '-(ET)₄H₃O[Fe(C₂O₄)₃] · (C₆H₄Br₂),

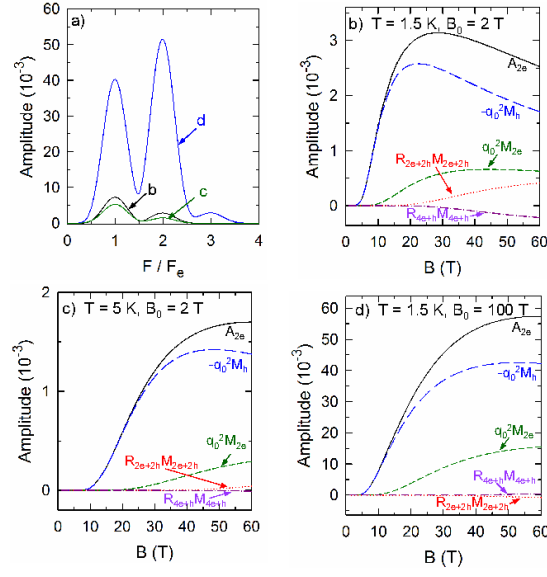


Fig. 3. (color on line) (a) Fourier spectra of the oscillatory magnetization calculated at a mean field of 40 T from Eq. 6 with $m_e = 1$, $m_h = 1$, $g_e^* = 2$, $g_h^* = 2$, $T_{De} = 1$ K, $T_{Dh} = 1$ K. Labels b, c, d correspond to $T = 1.5$ K and $B_0 = 2$ T, $T = 5$ K and $B_0 = 2$ T, $T = 1.5$ K and $B_0 = 100$ T, respectively. (b), (c), (d) Field dependence of the amplitude of the Fourier component with frequency $F_h = 2F_e$ corresponding to Labels b, c, d , respectively, of (a). Solid lines are calculated from Eq. 4. Long dashed, short dashed, dotted and dash-dotted lines are the components linked to the h , $2e$, $2e + 2h$ and $4e + h$ orbits, respectively. The magnetic breakdown damping factors for the orbits $2e + 2h$ and $4e + h$ are given by $R_{2e+2h} = 3p_0^4 q_0^2 - 2p_0^2 q_0^4$ and $R_{4e+h} = 2p_0^2 q_0^4 - 3p_0^4 q_0^2$, where q_0 and p_0 are the reflection and magnetic breakdown probability, respectively.

the FS of which (see Fig. 1(b)) is relevant to the above calculations. Note that this FS can be considered as resulting from the hybridization of a series of ellipses centered at the Γ point. The area of these ellipses, which is related to the total number of holes per unit cell in the HOMO bands, is twice the area of the cross section of the

FBZ because the repeat unit of the layer contains eight ET molecules with an average charge of $+1/2$, i.e. a total of four electrons per repeat unit. It is interesting to point out how this FS differs from that of other α -type ET salts, such as the α -(ET) $_2$ [MHg(SCN) $_4$] family. As pointed out by Mori et al. [18], the closed and open portions of the

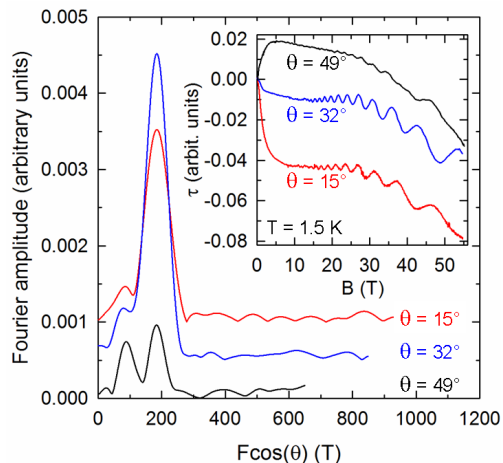


Fig. 4. Fourier analysis in the field range 25-55 T of the magnetic torque data reported in the insert for various directions of the magnetic field with respect to the normal to the conducting plane (angle θ).

latter can also be considered to arise from the hybridization of a series of ellipses with an area equal to the cross section of the first Brillouin zone (FBZ) and centered at Y (using the axes notation of Fig. 1(b)). Since the repeat unit of these salts contains only four ET molecules, the FS of Fig. 1(b) is just a folded version along the b^* direction of such FS. The different kind of overlap of the ellipses generated by the folding thus leads to the very different FS for the present salt (referred to as case (ii) above) and that of the α -(ET) $_2$ [MHg(SCN) $_4$] family (referred to as case (i) above).

Field-dependent magnetic torque data and corresponding Fourier analysis are reported in Fig. 4. Angle dependence of the two observed frequencies (not shown) follows the cosine law predicted for a 2D FS with $F_h(\theta = 0) = 183 \pm 3$ T and $F_e(\theta = 0) = 91 \pm 5$ T. Consistently with the FS topology reported in Fig. 1(b), they correspond to

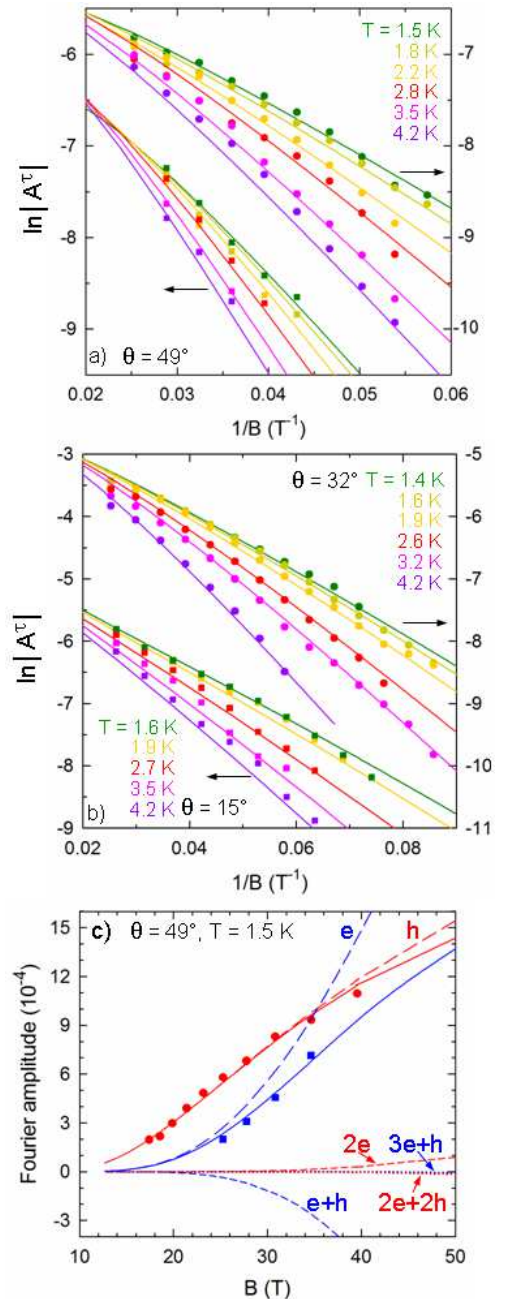


Fig. 5. $\ln(|A^\tau|)$ vs $1/B$ at various temperatures for (a) A_h^τ (solid circles) and A_e^τ (solid squares) at $\theta = 49^\circ$, (b) A_h^τ at $\theta = 15^\circ$ (solid squares) and 32° (solid circles) and (c) field dependence of A_h^τ (solid circles) and A_e^τ (solid squares) at $\theta = 49^\circ$ at 1.5 K. Solid lines are fits of Eqs. 7, obtained with $m_e = 0.93$, $m_h = 0.88$, $g_e^* = 2.27$, $g_h^* = 2.06$, $T_{De} = 5$ K, $T_{Dh} = 4$ K and $B_0 = 2$ T. Long dashed, short dashed, dotted and dash-dotted lines in (c) are the contributions of the various components entering the fittings (see text and Fig. 3).

the hole and electron orbits cross section area $S_h = 8.9 \pm 0.2 \%$ and $S_e = 4.4 \pm 0.3 \%$, respectively, of the FBZ area. These data are in agreement with magnetoresistance data ($S_h = 8.9 \%$ of the FBZ area) and band structure calculations at room temperature ($S_h = 7.6 \%$ of the FBZ area and $S_e = S_h/2$) [13]. Compared to the Fourier component with the frequency F_h , that with the frequency F_e , which was not observed in Ref. [13], has a relatively small amplitude at $\theta = 15^\circ$ and 32° , and can only be reliably studied at $\theta = 49^\circ$.

It must be noticed that the studied compound contains magnetic Fe^{3+} ions. As reported in the case of λ -(BETS) $_2\text{FeCl}_4$ (where BETS stands for bis-ethylenedithio-tetraselenafulvalene) [19,20], these magnetic ions induce an exchange field leading to angle-dependent splitting of the oscillation frequency which may alter the oscillations amplitude. Nevertheless, such a splitting is not observed neither in the considered compound nor in the compound with the same composition and β'' structure in fields of up to 55 T [21,22,23]. This could be due to the lower, by a factor of two, Fe^{3+} concentration in the present case hence to a reduced exchange coupling constant.

A naive analysis of the temperature dependence of A_h^τ , relevant to F_h , assuming that only one orbit contributes (i.e. through Eq. 1) yields an effective mass $m_h(\theta) \times \cos(\theta)$ of 0.96 ± 0.05 , 0.93 ± 0.02 and 0.69 ± 0.07 at $\theta = 15^\circ$, 32° and 49° , respectively. Within the same hypothesis, the magnetoresistance data at $\theta = 0^\circ$ of Ref. [13] yield $m_h = 1.11 \pm 0.04$ [24]. In other words, the product $m_h(\theta) \times \cos(\theta)$ would monotonously decrease as θ increases. Hence,

at variance with the angle dependence of the frequency, the cosine law ($m_h(\theta) = m_h(0)/\cos(\theta)$) consistent with a 2D FS, would not be followed for the effective mass within this assumption. This result strongly suggests that Eq. 1 is unable to account for the temperature dependence of the amplitude. Besides, it can be checked that the field dependence of the amplitude cannot be accounted for by Eq. 1 as well. As discussed in the preceding section and reported hereafter, other orbits (such as $2e$, $2e + 2h$, *etc.*) with effective masses different from each other enter the oscillatory spectra.

According to Eqs. 6, oscillatory torque amplitudes A_e^τ and A_h^τ , of the Fourier components with frequencies F_e and $F_h = 2F_e$ observed in Fig. 4, are given by:

$$A_e^\tau = \tau_0 \tan(\theta) B \frac{F_e}{\pi} A_e, \quad A_h^\tau = \tau_0 \tan(\theta) B \frac{2F_e}{\pi} A_{2e}, \quad (7)$$

respectively, where τ_0 is a prefactor depending on the cantilever stiffness, crystal geometry, *etc.* and θ is the angle between the field direction and the normal to the conducting plane. Amplitudes A_e and A_{2e} in Eqs. 7 are given by Eqs. 3 and 4, respectively. We will limit ourselves to small n_h and n_e values. Namely, in addition to the basic electron and hole orbits, only the second harmonic of the electron orbit ($2e$) and the MB orbits composed of one hole and one electron orbit ($e + h$), 3 electron and one hole orbits ($3e + h$), 2 electron and 2 hole orbits ($2e + 2h$) and 4 electron and one hole orbits ($4e + h$) are taken into account. In short, the contribution of the MB orbits and harmonics composed of more than 5 individual orbits are neglected. It must be kept in mind that spin damping fac-

tors may influence the sign of a given contribution or, in other words, induce a π dephasing, as observed on either side of a spin zero angle [5].

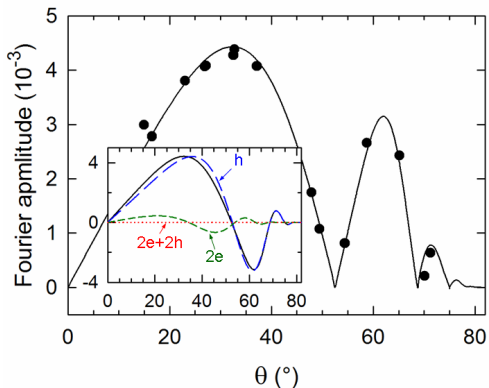


Fig. 6. Angle dependence of the amplitude $|A_h^\tau|$ at $T = 1.5$ K and $B = 40$ T. Solid line is the best fit of Eq.7 to the data, obtained with the same set of parameters as in Fig. 5. Long dashed, short dashed and dotted lines in the insert are the contributions of h , $2e$ and $2e + 2h$, respectively.

Fig. 5 displays field dependence at various temperatures of either A_e^τ or A_h^τ for $\theta = 15^\circ$ and 32° (crystal #1) and 49° (crystal #2) while Fig. 6 displays the angle dependence of A_h^τ at $T=1.5$ K and $B = 40$ T for crystal #2. Solid lines in these figures are the best fits of Eqs. 7 to the Fourier amplitudes: the same set of parameters stands for all the data, namely $m_e = 0.93 \pm 0.04$, $m_h = 0.88 \pm 0.04$, $g_e^* = 2.27 \pm 0.12$, $g_h^* = 2.06 \pm 0.09$. Dingle temperatures and MB field, which jointly govern the field dependence of the amplitude are obtained with a large uncertainty. Dingle temperatures are rather large, of the order of few K, whereas B_0 is in the range between 0 and 4 T which is rather small, in agreement with the FS of Fig. 1. Owing to the small size of e and h orbits, compared to that of

the FBZ, effective mass values are large which suggests significant renormalization due to many-body effects.

According to Dharma-wardana et al. [25], electron correlations are predicted to yield large Landé factor. Consistently, large values are observed, although they are within the spread range usually reported for organic metals [4]. In that respect, puzzling data can be found in the literature since, for example, values as small as $g_\alpha^* = 1.6$ and $g_\beta^* = 1.5$ are observed for the strongly correlated κ -(ET) $_2$ Cu(SCN) $_2$ compound [26]. Oppositely values larger than 2 are reported for e.g. κ -(ET) $_2$ I $_3$ ($g_\beta^* = 2.27$ [27]).

Composites orbits, $e + h$ and $2e$ have significant contributions to A_e^τ and A_h^τ , respectively, as observed in Fig. 5(c). Nevertheless, higher order terms (linked to $2e + 2h$ and $3e + h$) are small, due to rather large Dingle temperatures. Finally, as reported in Fig. 5c for the data at 49° , contributions of e and $3e + h$ to A_e have opposite signs. This result which also holds at 15° and 32° , explains why this amplitude is small compared to A_h^τ .

5 Summary and conclusion

Fourier spectra of de Haas-van Alphen oscillations of compensated two-dimensional metals with Fermi surface composed of one hole and two electron components have been considered. The two main Fourier components observed have frequencies F_e and $F_h = 2F_e$, corresponding to the electron and hole orbits area. Nevertheless, it is demonstrated that, taking into account the opposite sign of electron and hole orbits, a given Fourier component involves combination of several orbits, the contribution of which

must be included in the calculations. Such FS, which is a textbook case, is observed in the strongly 2D organic metal α -'pseudo- κ '-(ET)₄H₃O[Fe(C₂O₄)₃](C₆H₄Br₂). Magnetic torque oscillations of this compound have been studied up to 55 T for various directions of the magnetic field with respect to the conducting plane. It is demonstrated that data analysis performed assuming that only single electron and single hole orbits contribute to Fourier components with frequency F_e and $2F_e$, respectively, cannot account for the data. In other words, additional orbits generated by tunneling and reflection at magnetic breakdown junctions must be taken into account. Calculations are in good quantitative agreement with the data.

This work has been supported by EuroMagNET II under the EU Contract No. 228043, and MINECO-Spain (Projects FIS2012-37549-C05-05 and CSD 2007-00041).

References

1. R. Rousseau, M. Gener and E. Canadell, *Adv. Func. Mater.* **14**, 201 (2004).
2. A. B. Pippard, *Proc. Roy. Soc. (London)* **A270** 1 (1962).
3. D. Shoenberg, *Magnetic Oscillations in Metals* (Cambridge University Press, Cambridge, 1984).
4. J. Wosnitza, *Fermi Surfaces of Low-Dimensional Organic Metals and Superconductors*, Springer Tracts in Modern Physics **134** (1996).
5. J. Singleton, *Rep. Prog. Phys.* **63** 1111 (2000).
6. A. Audouard and J.-Y. Fortin, *C. R. Physique* **14** 15 (2013).
7. J.-M. Carter, D. Podolsky and H.-Y. Kee, *Phys. Rev. B* **81** 064519 (2010).
8. T. Helm, M.V. Kartsovnik, I. Sheikin, M. Bartkowiak, F. Wolff-Fabris, N. Bittner, W. Biberacher, M. Lambacher, A. Erb, J. Wosnitza and R. Gross, *Phys. Rev. Lett.* **105** 247002 (2010).
9. T. Helm, M. V. Kartsovnik, C. Proust, B. Vignolle, C. Putzke, E. Kampert, I. Sheikin, E.-S. Choi, J. S. Brooks, N. Bittner, W. Biberacher, A. Erb, J. Wosnitza, and R. Gross, arXiv:1403.7398
10. J.-Y. Fortin and A. Audouard, *Phys. Rev. B* **77** 134440 (2008).
11. J.-Y. Fortin and A. Audouard, *Phys. Rev. B* **80** 214407 (2009).
12. S. S. Khasanov, B. Zh. Narymbetov, L. V. Zorina, L. P. Rozenberg, R. P. Shibaeva, N. D. Kushch, E. B. Yagubskii, R. Rousseau and E. Canadell, *Eur. Phys. J. B* **1** 419 (1998).
13. L. V. Zorina, S. S. Khasanov, S. V. Simonov, R. P. Shibaeva, V. N. Zverev, E. Canadell, T. G. Prokhorova and E. B. Yagubskii, *Cryst. Eng. Comm.* **13** 2430 (2011).
14. L. V. Zorina, S. S. Khasanov, S. V. Simonov, R. P. Shibaeva, P. O. Bulanchuk, V. N. Zverev, E. Canadell, T. G. Prokhorova and E. B. Yagubskii, *Cryst. Eng. Comm.* **14** 460 (2012).
15. P.D. Grigoriev, M.V. Kartsovnik, W. Biberacher, N.D. Kushch and P. Wyder *Phys. Rev. B* **65** 060403(R) (2002).
16. L. M. Falicov and H. Stachowiak, *Phys. Rev.* **147** 505 (1966)
17. R.G. Chambers, *Proc. Phys. Soc.* **88** 701 (1966).
18. H. Mori, S. Tanaka, M. Oshima, G. Saito, T. Mori, Y. Maruyama and H. Inokuchi, *Bull. Chem. Soc. Jpn.* **63** 2183 (1990)

19. S. Uji, C. Terakura, T. Terashima, T. Yakabe, Y. Terai, M. Tokumoto, A. Kobayashi and F. Sakai, Phys. Rev. B **65** 113101 (2002).
20. O. Cépas, Ross H. McKenzie and J. Merino, Rev. B **65** 100502 (2002).
21. D. Vignolles, A. Audouard, V.N. Laukhin, E. Canadell, T.G. Prokhorova and E.B. Yagubskii, Eur. Phys. J. B **203** 489 (2009).
22. D. Vignolles, A. Audouard, V.N. Laukhin, E. Canadell, T.G. Prokhorova and E.B. Yagubskii, Synth. Met. **160** 2467 (2010).
23. V. N. Laukhin, A. Audouard, D. Vignolles, E. Canadell, T. G. Prokhorova and E. B. Yagubskii, Low Temp. Phys. **37** 749 (2011).
24. The, even larger, effective mass value $m_h = 1.26$, reported in Ref. [13] is deduced from a high temperature asymptotic approximation of the temperature damping factor.
25. M. W. C. Dharma-wardana, Phys. Rev. B **72** 125339 (2005).
26. V. M. Gvozdkov, Y. V. Pershin, E. Steep, A. G. M. Jansen and P. Wyder, Phys. Rev. B **65** 165102 (2002).
27. M. Heinecke, K. Winzer, D. Schweitzer, Z. Phys. B **93** 45 (1993).

